Origin of Ultrastability in Vapor-Deposited Glasses

Ludovic Berthier, Patrick Charbonneau, Elijah Flenner, and Francesco Zamponi

Phys. Rev. Lett. **119**, 188002 — Published 1 November 2017

DOI: 10.1103/PhysRevLett.119.188002

The origin of ultrastability in vapor-deposited glasses

Ludovic Berthier,[1] Patrick Charbonneau,[2] Elijah Flenner,[3] and Francesco Zamponi[4]

[1] *Laboratoire Charles Coulomb, UMR 5221, Université de Montpellier and CNRS, 34095 Montpellier, France*
[2] *Department of Chemistry, Duke University, Durham, NC 27708;*
Department of Physics, Duke University, Durham, NC 27708
[3] *Department of Chemistry, Colorado State University, Fort Collins, CO 80523*
[4] *Laboratoire de physique théorique, Ecole normale supérieure, PSL Research University, Sorbonne Universités, UPMC Univ. Paris 06, CNRS, 75005 Paris, France*

(Dated: August 14, 2017)

Glass films created by vapor-depositing molecules onto a substrate can exhibit properties similar to those of ordinary glasses aged for thousands of years. It is believed that enhanced surface mobility is the mechanism that allows vapor deposition to create such exceptional glasses, but it is unclear how this effect is related to the final state of the film. Here we use molecular dynamics simulations to model vapor deposition and an efficient Monte Carlo algorithm to determine the deposition rate needed to create ultra-stable glassy films. We obtain a scaling relation that quantitatively captures the efficiency gain of vapor deposition over bulk annealing, and demonstrates that surface relaxation plays the same role in the formation of vapor-deposited glasses as bulk relaxation does in ordinary glass formation.

Compared to their liquid-cooled counterparts, vapor-deposited glasses have a higher density [1], a higher kinetic stability [2–4], and a lower heat capacity [5]. This makes them promising materials for a wide range of applications, such as drug delivery [6], protective coatings [7, 8], and lithography [9]. Identifying the microscopic process that gives rise to these properties is thus crucial to designing novel amorphous materials [10]. Vapor deposition indeed does not systematically result in glasses with improved characteristics. It is observed that the substrate ought to be held at a specific temperature (around 85% of the glass transition temperature T_g of the liquid [3]) and that the deposition rate must be sufficiently slow [11] to get optimal films. A microscopic explanation for the optimality of $0.85T_g$, and an estimate of what is a "sufficiently slow" deposition rate are, however, still lacking. Moreover, while simulations and experiments have shown that vapor-deposited glasses may lie lower in the potential energy landscape than liquid-cooled glasses [3, 11–16], and sometimes have the same structure as glasses of a comparable energy [14], it is not known whether vapor deposition can provide truly equilibrium configurations, especially below T_g.

Here we provide a quantitative test of the role of surface mobility in the creation of vapor deposited glasses. More specifically, we answer two key questions. *(i)* How much more efficient is vapor deposition than standard cooling in creating a glass or, more precisely, given a substrate temperature and a deposition rate, what is the effective cooling rate that would produce the same configurations? *(ii)* What is the deposition rate needed to produce fully equilibrated configurations? Answering these questions is a challenging program that requires characterizing equilibrated films at temperatures sufficiently low for a large difference between surface and bulk relaxation to have developed, as well as measuring bulk and surface dynamics in a same material, over the same temperature range, and under the same thermodynamic conditions. We overcome these problems by using, on a properly chosen polydisperse Lennard-Jones model, a swap Monte Carlo algorithm that efficiently samples the energy landscape at very low temperatures, speeding up equilibration by several orders of magnitude over standard molecular dynamics [17, 18]. This allows us to compare free standing equilibrated films with those grown on an equilibrated substrate using an algorithm that closely mimics experimental vapor deposition, and to independently determine the low temperature equilibrium energy

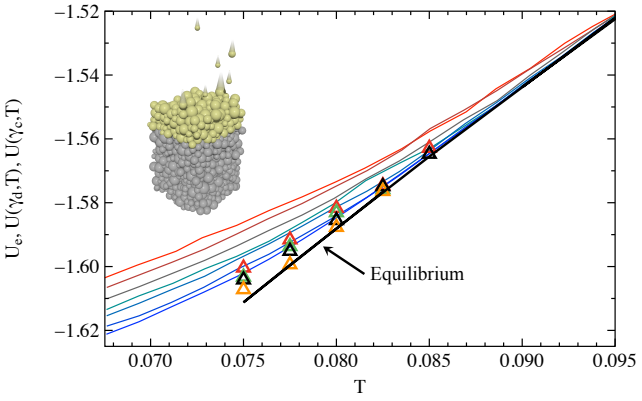

FIG. 1. Average potential energy for ordinary liquid-cooled films (lines) for cooling rates of $\gamma_c = 10^{-5}$, 5×10^{-6}, 2×10^{-6}, 10^{-6}, 5×10^{-7}, 2×10^{-7}, and 10^{-7} listed from top to bottom. The open triangles are for vapor-deposited films with deposition rates $\gamma_d = 2.2{\times}10^{-3}$ (red), $7.3{\times}10^{-4}$ (green), $2.2{\times}10^{-4}$ (black), and 4.4×10^{-5} (orange). The black line is the potential energy for the equilibrium supercooled liquid film. Inset: illustration of the vapor deposition with the growing film (red particles) and a temperature-controlled substrate (green particles).

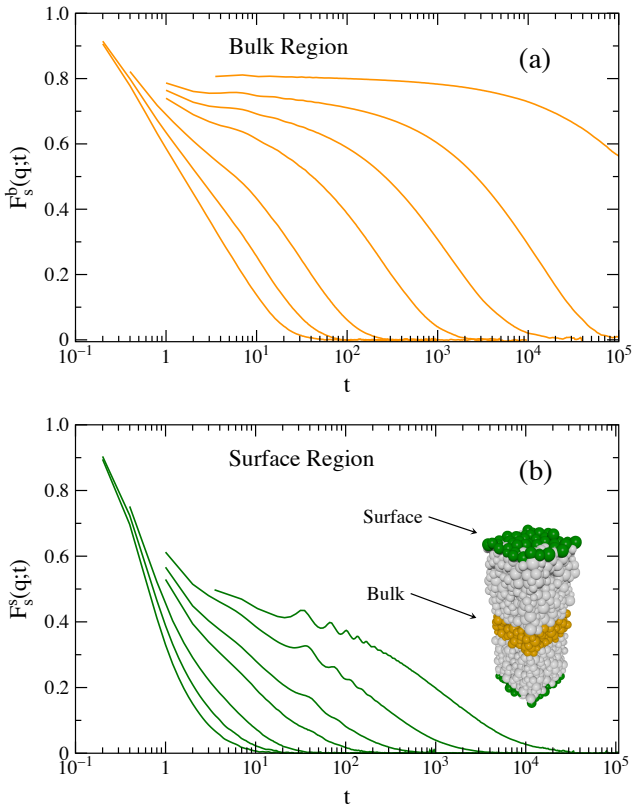

FIG. 2. (a) Self-intermediate scattering function calculated for particles initially within the core region of an equilibrated supercooled liquid film, $F_s^b(\mathbf{q};t)$, for $T = 0.12$, 0.11, 0.1, 0.09, 0.085, 0.08, and 0.075, from left to right. (b) Self-intermediate scattering function calculated for particles initially at the film surface, $F_s^s(\mathbf{q};t)$, for the same temperatures. The inset illustrates the extent of the surface and the core regions of an equilibrium freestanding film.

of the film with no extrapolation.

We simulate a polydisperse mixture of Lennard-Jones particles with interaction potential, $V(r_{ij}) = \epsilon\left[(\sigma_{ij}/r_{ij})^{12} - (\sigma_{ij}/r_{ij})^{6}\right]$, which is truncated and shifted to zero at $2.5\sigma_{ij}$. The size parameter σ_{ij} is given by a non-additive mixing rule $\sigma_{ij} = 0.5(\sigma_i+\sigma_j)(1-\Delta|\sigma_i-\sigma_j|)$, where $\Delta = 0.2$. The mixing parameter Δ is chosen to avoid separation of the particles into small and large components at low pressures and temperatures [18]. The particle size parameter σ is chosen from the probability distribution $P(\sigma) = A/\sigma^3$ for $0.73 \leq \sigma \leq 1.62$ and zero otherwise [18]. For each temperature we simulate five different realizations of the size distribution. Each particle has the same mass m, the unit of energy is ϵ, and the unit of length is the average of the particle diameters σ_0. Our unit of time is $\sqrt{\sigma_0^2 m/\epsilon}$. The freestanding films have box lengths of $11\sigma_0$ in the periodic x and y directions. The box length in the z direction is $120\sigma_0$. We simulate systems of $N = 4000$ particles, which results in films of around $30\sigma_0$ along the z direction.

To create equilibrium free standing films we used a Monte Carlo swap algorithm. The algorithm consists of two Monte Carlo moves, a standard attempted displacement move and an attempted swap move. For the attempted displacement move we use trial positions within a cube of side d, where d is adjusted for each temperature so that the acceptance rate lies between 0.3 to 0.35. For the attempted swap move we consider exchanging the size of two particles chosen at random. The move type is chosen at random, with 20% of the moves being attempted swaps.

For the vapor-deposited films we first create an equilibrated substrate of the same system with $N/2 = 2000$ particles in a simulation box of the same dimensions as for the free-standing film. We then introduce $N/2$ particles with x and y components of the velocity randomly chosen within the square of side 0.02. The z plane from which particles are introduced moves at a constant velocity in order to remain about $40\sigma_0$ above the surface of the substrate. The velocity of the deposited particles in the z direction has a magnitude corresponding to a kinetic temperature of $T = 0.1$ (the onset temperature of slow dynamics), directed towards the substrate. The total momentum of the whole system is set to zero at every time step to reduce the drift of the center of mass. The substrate is simulated using a Nosé-Hoover constant NVT algorithm, and the vapor-deposited particles are simulated using a constant NVE algorithm. After all the particles are deposited onto the substrate, the simulation is run for $t = 100$ and the following $t = 1000$ is used to calculate the average energy for that deposition rate. In all cases the energy changes little over the averaging window.

Figure 1 compares the temperature evolution of the average potential energy, U, measured in the exact same film geometry and at the same temperature T for three different protocols. Vapor-deposited films at deposition rate $\gamma_d = dz/dt$ and substrate temperature T have energy $U(\gamma_d, T)$ (triangles), ordinarily-cooled films at cooling rate $\gamma_c = dT/dt$ have energy $U(\gamma_c, T)$ (colored lines), and films equilibrated using swap Monte Carlo have energy $U_e(T)$ (black line). In agreement with prior experiments and simulations [13, 14, 16], the results show that vapor deposition equilibrates our model more efficiently than liquid cooling for a comparable preparation time, especially at low temperatures. The average energy obtained at slower cooling rates indeed deviates from equilibrium below $T \approx 0.085$, while the films grown by vapor deposition have energies much closer to equilibrium. For our slowest deposition rate, the average energy remains equal to the equilibrium energy for all but the lowest temperature studied, $T = 0.075$.

We are now in the position to answer the key questions raised in the introduction. For liquid-cooled films, the competition between the bulk relaxation time τ_α^b and the cooling rate γ_c controls the distance to equilibrium. This

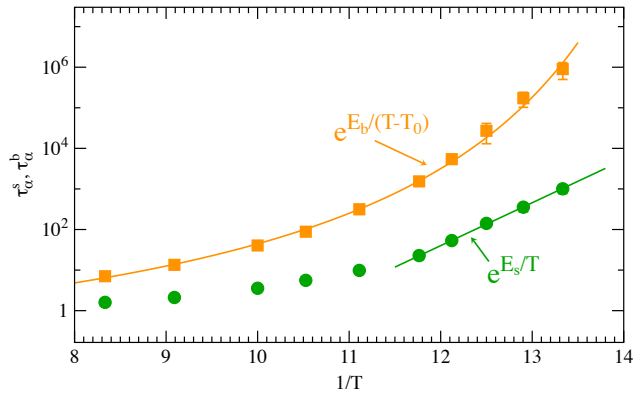

FIG. 3. The relaxation times for the bulk region τ_α^b (blue squares) and the surface region τ_α^s (red circles) both grow with decreasing temperature. The corresponding lines are fits to a Vogel-Fulcher fit, $\tau_\alpha^b = \tau_0^b e^{E_b/(T-T_0)}$ with $T_0 = 0.0612 \pm 0.001$, and an Arrhenius form, $\tau_\alpha^s = \tau_0^s e^{E_s/T}$.

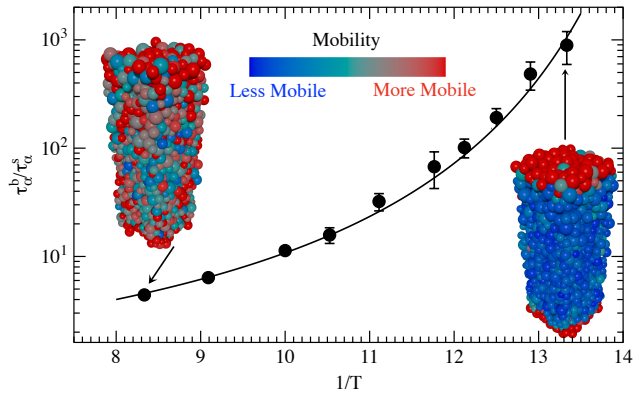

FIG. 4. The ratio $\tau_\alpha^b/\tau_\alpha^s$ grows rapidly with decreasing temperature. The line is an empirical fit to a Vogel-Fulcher form, $\tau_\alpha^b/\tau_\alpha^s \sim e^{E_r/(T-T_0)}$, with the same T_0 as for τ_α^b. The insets show particles at time $t = 0$ colored according to their displacement $20\tau_\alpha^s$ later. Red particles have moved more than one σ_0 and blue particles less than $0.5\sigma_0$. The left inset shows that at $T = 0.12$ particles within the core of the film move significantly over this timescale. The right inset shows the emergence of a very thin mobile surface layer at $T = 0.075$.

may be captured by the scaling relation

$$U(\gamma_c, T)/U_e(T) = \mathcal{C}(x_c), \tag{1}$$

where $x_c = \gamma_c \tau_\alpha^b(T)/T$ represents the (adimensional) ratio between cooling and bulk relaxation timescales. To establish that vapor-deposited films are controlled by the competition between the equilibrium relaxation time at the film surface τ_α^s and the deposition rate γ_d we seek a scaling relation of the same form,

$$U(\gamma_d, T)/U_e(T) = \mathcal{D}(x_d), \tag{2}$$

where $x_d = \gamma_d \tau_\alpha^s(T)/\sigma_0$ is the (adimensional) ratio between deposition and surface relaxation timescales and σ_0 is the average particle size. By construction, the scaling functions $\mathcal{C}(x)$ and $\mathcal{D}(x)$ should both converge to unity when $x \to 0$.

To test these scalings, we measure the temperature dependence of the *equilibrium* relaxation times at the film surface and in its core. To this end, we consider equilibrium films obtained from the swap Monte Carlo algorithm, that we then simulate using ordinary molecular dynamics. The measurements described in the following are thus generic for all films and are not specific to vapor-deposited ones.

Relaxation times are extracted from the decay of the self-intermediate scattering function $F_s^l(q;t) = (1/N_l)\sum_{n=1}^{N_l} e^{i\mathbf{q}\cdot[\mathbf{r}_n(t)-\mathbf{r}_n(0)]}$, where the sum is restricted to the N_l particles with positions $\mathbf{r}$ either in the bulk, $l = b$, or at the surface, $l = s$, of the film at time $t = 0$. The chosen wavevector, $|\mathbf{q}| = 7.1$, coincides with the location of the first peak of the static structure factor, and is taken parallel to the surface. The bulk region is defined to be $5\sigma_0$ thick at the core of a film approximately $30\sigma_0$ thick, while the two surface regions extend $1.5\sigma_0$ from the film edge, as illustrated in the inset of Fig. 2.

In Fig. 2(a), $F_s^b(\mathbf{q};t)$ appears typical of standard glassy dynamics [19]. A plateau emerges for $T \leq 0.1$, and both its length and height increase with decreasing temperature. Particles are thus localized over an increasingly longer timescale upon increased cooling. The $F_s^s(\mathbf{q};t)$ in Fig. 2(b) are markedly different. First, there is no distinct plateau at any temperature. Second, a fast initial decay down to ~ 0.5 is followed by a slower relaxation. This suggests that surface particles perform vibrational motion with a larger amplitude than bulk ones. More importantly, the long-time dynamics at the surface is much faster than in the core.

Defining the relaxation times as $F_s^l(q;\tau_\alpha^l) = 0.2$ gives a measure of the time needed for a particle to move a distance comparable to its diameter. Empirically, τ_α^b is well-described over the whole temperature range by a Vogel-Fulcher form $\tau_\alpha^b = \tau_0^b e^{E_b/(T-T_0)}$, with $T_0 = 0.0612 \pm 0.001$ (Fig. 3), but other fitting forms work equally well. The surface relaxation time τ_α^s also increases with decreasing temperature, although much less than τ_α^b, and a Vogel-Fulcher form does not fit it well. Instead, τ_α^s is better described by an Arrhenius form, $\tau_\alpha^s = \tau_0^s e^{E_s/T}$, at low temperatures, which is reminiscent of the behavior of surface diffusion observed experimentally [20–22]. As a result, the ratio $\tau_\alpha^b/\tau_\alpha^s$ increases dramatically upon supercooling, growing from ~ 4 near the onset of localization to ~ 900 at the lowest temperature studied (Fig. 4). Under the assumption (proved shortly below) that the surface relaxation time controls the thermalization of the vapor-deposited glass, then the much faster surface relaxation is qualitatively consistent with the enhanced thermalization efficiency of vapor deposition observed in Fig. 1.

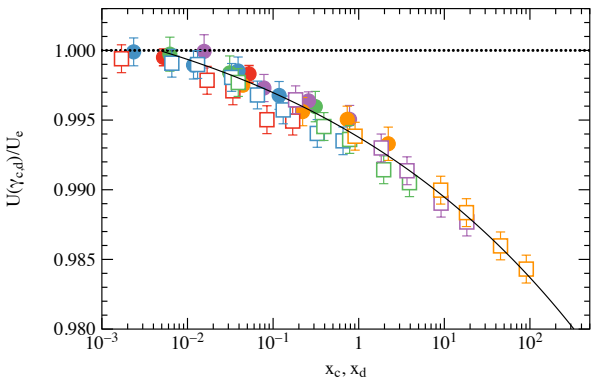

FIG. 5. The excellent collapse observed for $U(\gamma_{c,d}, T)/U_e$ as a function of $x_c = \gamma_c \tau_\alpha^b / T$ and $x_d = \gamma_d \tau_\alpha^s / \sigma_0$ for liquid-cooled films (squares), and vapor-deposited films (circles) indicates that surface relaxation plays the same role in the formation of vapor-deposited films as bulk relaxation in ordinary liquid-cooled film formation. Temperatures $T = 0.085$ (red), $T = 0.0825$ (blue), $T = 0.08$ (green), $T = 0.0775$ (purple), and $T = 0.075$ (orange). The solid line is an empirical fit.

To visualize the emergence of a mobile surface layer, we color particles according to their displacement $|\mathbf{r}_n(t) - \mathbf{r}_n(0)|$ after $t = 20\tau_\alpha^s$ for the highest and lowest temperature examined as insets to Fig. 4. At all temperatures the surface is more mobile than the core, but qualitative differences can be observed. At the highest temperature mobile particles are found throughout the film, while at the lowest temperature only a small layer of mobile particles is observed. This layer is barely thicker than σ_0 in the representation of Fig. 4. (Fitting an exponential decay to the surface relaxation time gradient, see Ref. [16], gives a thickness of order 2-3 σ_0 with a weak temperature dependence.) Such a decoupling between bulk and surface dynamics has been experimentally documented [23], but was not directly connected to the thermalization of ultrastable glasses before.

The mobile surface layer is exploited by the vapor-deposition process to speedup the thermalization of glassy films, as we can directly demonstrate. The combination in Fig. 5 of all our energy measurements in liquid-cooled and vapor-deposited films shows that Eqs. (1, 2) collapse the numerical results very well. Moreover, the simulations indicate that the scaling functions $\mathcal{C}(x)$ and $\mathcal{D}(x)$ are nearly identical. Note that no adjustable parameter is used for these scalings, which combine independent numerical measurements.

The excellent data collapse in Fig. 5 indicates that the surface relaxation time and deposition rate determine the distance to equilibrium for vapor-deposited films in the exact same way that bulk relaxation time and cooling rate control the distance from equilibrium for liquid-cooled films. This result suggests that one can convert the deposition rate of a film into an effective cooling rate as $\gamma_c^{\text{eff}} = \gamma_d(\tau_\alpha^s/\tau_\alpha^b)(T/\sigma_0)$. Quantitatively, we can fit the scaled data to an empirical power law, $\mathcal{P}(x) = ax^\nu + b$ (with $\nu = 0.12 \pm 0.03$, solid line in Fig. 5) [14]. Solving for $\mathcal{P}(x) = 1$ gives the maximal rate, for both preparation processes, at which equilibrium films can be prepared. Our simulations thus provide a simple quantitative criterion, $x_d = \gamma_d \tau_\alpha^s / \sigma_0 \leq 0.005$, to create equilibrium vapor-deposited films.

Consistency with experiments is illustrated by considering the case of indomethacin [3, 21], for which we use $\sigma_0 = 1$ nm [21] as the length unit and 10^{-12} s as the time unit [24]. We further approximate the structural relaxation times using $\tau_\alpha^l = (q^2 D^l)^{-1}$ at $q = 2\pi/\sigma_0$ with the diffusion coefficients D obtained in Ref. [21]. For a cooling rate of 40 K/min, Swallen *et al.* determined that $T_g = 315$ K [3]. We thus estimate that $\gamma_c \tau_\alpha^b(T_g)/T_g \approx 0.0054$, which is in close agreement with the above criterion. Our proposed scaling form, thus captures well the cooling rate dependence of the glass transition. More interestingly, we can compute the lowest temperature at which one can obtain an equilibrium film by vapor deposition for a given deposition rate. For $\gamma_d = 0.2$ nm/s [25], we estimate that the smallest surface diffusion coefficient at which an equilibrium film can be obtained should be $D^s \approx 1.0 \times 10^{-18}$ m^2/s. By extrapolating the surface diffusion coefficients in Ref. [25, Fig. 3], we find that an equilibrium vapor-deposited film should be accessible down to 264 K $\approx 0.84 T_g$, which is close to the experimental estimate [25]. Note that for simulations our results imply that an efficiency gain of at most 2-3 orders of magnitude can be expected from vapor deposition over standard bulk annealing, which appears consistent with a recent independent estimate [16]. In the regime accessible to experiments, by contrast, that gain can reach eight orders of magnitude.

Our work directly and quantitatively demonstrates how enhanced surface diffusion, as quantified by τ_α^s, is responsible for the ultrastability of vapor-deposited films. Additional considerations may be needed to account for the full scope of experimental observations. First, additional studies are needed to connect the surface relaxation time measured in this study with the surface mobility inferred from experiments [2, 3, 5, 21–23, 26]. Second, the shape and chemical nature of vapor-deposited molecules can result in preferential orientation within the vapor-deposited film [1, 13, 27–30], while such alignment bias is not expected for ordinary liquid-cooled films. Although molecular alignment can be used to tailor glassy properties [29, 30], it also inherently leads to vapor-deposited films that differ in structure from their liquid-cooled counterpart. For the simple, spherical particles studied in this work, however, we find no evidence in the pair-correlation function (not shown) or the density profile that vapor deposition produces different structures or particle segregation profiles than what is seen in liquid cooling. Our results are thus consistent with those of Reid *et al.* [14] for a binary Lennard-Jones system. Over-

all, this work is a first step to obtain a more quantitative understanding of the creation of vapor deposited supercooled liquids and glasses, and additional work is needed to understand the role of the substrate, molecular shape, and other factors in this process.

E.F. acknowledges funding from NSF DMR-1608086. This work was supported by a grant from the Simons Foundation (#454933 Ludovic Berthier, #454937 Patrick Charbonneau, #454955 Francesco Zamponi). We thank Mark Ediger, Beatriz Seoane, and Grzegorz Szamel for many useful discussions.

[1] S.S. Dalal, A. Sepúlveda, G.K. Pribil, Z. Fakhraai and M.D. Ediger, J. Chem. Phys. **136**, 204501 (2012).
[2] C. Rodríguez-Tinoco, J. Ràfols-Ribé, M. González-Silveira, and J. Rodríguez-Viejo, Sci. Rep. **6**, 35607 (2016).
[3] S.F. Swallen, K.L. Kearns, M.K. Mapes, Y.S. Kim, R.J. McMahon, M.D. Ediger, T. Wu, L. Yu, and S. Satija, Science **315**, 353 (2007).
[4] E. Leon-Gutierrez, A. Sepulveda, G. Garcia, M.T. Clavaguera-Mora, and J. Rodríguez-Viejo, Phys. Chem. Chem. Phys. **12**, 14693 (2010).
[5] K.L. Kearns, M.D. Ediger, H. Huth, and C. Schick, J. Phys. Chem. Lett. **1**, 388 (2010).
[6] B.C. Hancock and G. Zografi, J. Pharm. Sci. **86**, 1-12 (1997).
[7] H.B. Yu, Y.S. Luo, K. Samwer, Adv. Materials **25**, 5904 (2013).
[8] J.P. Chu, J.S.C. Jang, J.C. Huang, H.S. Chou, Y. Yang, J.C. Ye, Y.C. Wange, J.W. Lee, F.X. Liu, P.K. Liaw, Y.C. Chen, C.M. Lee, C.L. Li, and C. Rullyani, Thin Solid Films **520**, 5097 (2012).
[9] C. Neuber, A. Ringk, T. Kolb, F. Wieberger, P. Strohriegl, H.-W. Schmidt, V. Fokkema, M. Cooke, C. Rawlings, U. Drig, A.W. Knoll, J.-F. de Marneffe, P. De Schepper, M. Kaestner, Y. Krivoshapkina, M. Budden, I.W. Rangelow, *SPIE Advanced Lithography*, edited by D. Resnick and C. Bencher (International Society for Optics and Photonics, 2014), 90491V.
[10] L. Berthier and M. D. Ediger, Physics Today **69**, 40 (2016).
[11] Y.Z. Chua, M. Ahrenberg, M. Tylinski, M.D. Ediger, and C. Schick, J. Chem. Phys. **142**, 054506 (2015).
[12] I. Lyubimov, M.D. Ediger, and J.J. de Pablo, J. Chem Phys. **139**, 144505 (2013).
[13] I. Lyubimov, L. Antony, D.M. Walters, D. Rodney, M.D. Ediger, and J.J. de Pablo, J. Chem. Phys. **143**, 094502 (2015).
[14] D.R. Reid, I. Lyubimov, M.D. Ediger, and J.J. de Pablo, Nat. Commun. **7**, 13062 (2016).
[15] S. Singh and J.J. de Pablo, J. Chem. Phys. **134**, 194903 (2011).
[16] W. Zhang, J.F. Douglas, and F.W. Starr, J. Chem. Phys. **146**, 203310 (2017).
[17] L. Berthier, D. Coslovich, A. Ninarello, and M. Ozawa, Phy. Rev. Lett. **116**, 238002 (2016).
[18] A. Ninarello, L. Berthier, and D. Coslovich, arXiv:1704.08864.
[19] L. Berthier and G. Biroli, Rev. Mod. Phys. **83**, 587 (2011).
[20] Z. Yang, Y. Fujii, F. K. Lee, C.-H. Lam, and O. K. C. Tsui, Science **328**, 1676 (2010).
[21] L. Zhu, C.W. Brian, S.F. Swallen, P.T. Straus, M.D. Ediger, and L. Yu, Phys. Rev. Lett. **106**, 256103 (2011).
[22] C.R. Daley, Z. Fakhraai, M.D. Ediger, and J.A. Forrest, Soft Matter **8**, 2206 (2012).
[23] Y. Zhanga and Z. Fakhraai, PNAS USA **114**, 4915-4919 (2017).
[24] T.-X. Xiang and B.D. Anderson, Mol. Pharmaceutics **10**, 102-114 (2013).
[25] S.S. Dalal, Z. Fakhraai, and M.D. Ediger, J. Phys. Chem. B **117**, 15415 (2013).
[26] R. Malshe, M.D. Ediger, L. Yu, and J.J. de Pablo, J. Chem. Phys. **134**, 194704 (2011).
[27] D. Yokoyama, A. Sakaguchi, M. Suzuki, C. Adachi, Org. Electron. **10**, 127 (2009).
[28] D. Yokoyama and C. Adachi, J. Appl. Phys. **107**, 123512 (2010).
[29] S.S. Dalal, D.M. Walters, I. Lyubimov, J.J. de Pablo, and M.D. Ediger, PNAS **112**, 4227 (2015).
[30] J. Jiang, D.M. Walters, D. Zhou, and M.D. Ediger, Soft Matter **12** 3265 (2016).